

# Investigation of the applicability of post-irradiation annealing to reduce the degree of disorder in AlN ceramic to proton irradiation

A.L. Kozlovskiy<sup>1,2</sup>

<sup>1</sup>Laboratory of Solid State Physics, The Institute of Nuclear Physics, Almaty, Kazakhstan

<sup>2</sup>Engineering Profile Laboratory, L.N. Gumilyov Eurasian National University, Nur-Sultan, Kazakhstan

E-mail: kozlovskiy.a@inp.kz

DOI: 10.29317/ejpfm.2020040403

Received: 05.10.2020 - after revision

The work presents study results of the applicability of high-temperature heat treatment (500-700°C) of nitride ceramics irradiated with protons with an energy of 1.5 MeV and a dose of  $10^{16} \text{ cm}^{-2}$ . It was found that heat treatment for 60 minutes at a temperature of 700°C allows us to significantly reduce the density of radiation-induced defects and distortions in ceramics structure due to partial annihilation and relaxation of point defects. Dependences of changes in the strength and mechanical characteristics of ceramics on the temperature of post-irradiation annealing are shown. Based on the data obtained, a conclusion was made about prospects of using post-irradiation annealing to maintain the strength of ceramics subjected to loading during operation.

**Keywords:** proton irradiation, radiation-resistant ceramics, aluminum nitride, deformation, strength and wear resistance.

## 1. Introduction

In modern materials science of structural materials, one of the promising tasks is to find a solution to the problem of wear resistance and strength of materials during operation under the influence of ionizing radiation [1-3]. The problem is based on partial destruction of the surface layer; it's cracking or peeling as a result of defects accumulation during irradiation, also in the case of friction or sliding.

For structural materials for nuclear energy of new generation reactors, the use of ceramic materials based on nitrides, carbides or oxides leads to a significant increase not only in temperature variations in operating conditions, but also in a significant increase in the operation life [4, 5]. Interest in ceramic materials for new generation reactors is caused by their physical-chemical properties, high melting point, which in most cases exceeds 1500-2500°C, low reactivity to aggressive media, acids or alkaline solutions, high resistance to various types of ionizing radiation [6-10]. Particularly, ceramics based on aluminum nitride showed high resistance to helium swelling and irradiation with ions comparable in magnitude to fission fragments of uranium nuclei [11-13].

Formation of gas inclusions and regions with an increased concentration of defects [14, 15] are observed when exposed to light gas ions, such as helium, carbon or protons, which have poor solubility, high mobility, the ability to implant and subsequent agglomeration in the structure of surface layer at high irradiation doses. In this case, the hexagonal type of crystal structure leads to an uneven distribution of these defective regions in the structure. The uneven distribution of defects in the structure can lead to an increase in overstrain and distortions in the structure, which subsequently negatively affects the operation properties of ceramics [16-18].

One of the ways to control hydrogenation and swelling in ceramics is high-temperature rapid annealing, which partially reduces the concentration of defects in the structure due to their temperature relaxation [19, 20].

The AlN ceramics selected as investigated object are one of the promising ceramic materials in microelectronics and optical devices [21, 22], dosimetry of ionizing radiation [23, 24], insulating materials with high thermal conductivity used in nuclear and fusion energy [25, 26]. Aluminium nitride possesses high values of thermal conductivity, mechanical strength, resistance to degradation in aggressive environments, and good insulating properties. The high radiation resistance to various types of ionizing radiation is evidenced by a large number of scientific works in studying the mechanisms of defect formation in ceramics under irradiation, including the effect of electrons and gamma radiation [22], neutron irradiation [27, 28], irradiation with heavy ions [29, 30]. The high resistance to radiation effects is due to the crystal structure of aluminum nitride, and the high value of the threshold displacement energy  $> 34$  keV/nm. Also, at the moment there is no direct evidence of the presence of ion tracks in AlN ceramics under ion irradiation, which also indicates a high resistance to irradiation of this type of ceramics, comparable to SiC ceramics [31]. However, there are not so many works on studying the effect of irradiation with protons, and processes of hydrogen absorption and subsequent structural changes [32-35]. In most cases, proton irradiation doses are  $10^{12}$ - $10^{15}$  ion/cm<sup>2</sup>, which can lead to a significant change in point defects concentration and their mobility in the structure. The high penetrating ability of protons and the high energy of protons can lead, firstly, to a change in the electron density along the trajectories of motion, which leads to a change in the density of defects, and structural changes [35]. In this case, in the case of irradiation with protons, the main role in defects creation is played by point defects, vacancies, dislocations, an increase in the density of which leads to

structural disordering in ceramics.

The aim of this work is to study the effect of post-radiation annealing on the change in structural and strength characteristics of AlN ceramics irradiated with protons at a dose of  $10^{16} \text{ cm}^{-2}$ , which is characteristic of the overlapping effect of defect regions, and the creation of significant structural changes. One of the ways to reduce the concentration of point defects is the method of post-radiation thermal annealing. Particularly, this method has proven itself well in studies of changes in the concentration of F centers arising from irradiation with electrons, neutrons, protons, and heavy ions in ceramics and crystals [36-42].

However, it should be noted that thermal annealing allows annealing of defects in the entire volume of the sample, which for some cases is technically impossible or unacceptable. In this case, methods of laser destruction of defects are used, which makes it possible to anneal the defects locally [43-45].

## 2. Experimental part

### 2.1 Initial samples

Polycrystalline aluminum nitride ceramics with a wurtzite-type crystal structure manufactured by Shenzhen JRFT were used as investigated samples. These ceramics have a high melting point and thermal conductivity, a degree of structural ordering in the initial state of 97.6%, according to X-ray diffraction analysis. Before the irradiation, the ceramics were subjected to a series of successive grinding and polishing operations using grinding wheels with different grain sizes, and a polishing diamond paste. The average value of the degree of roughness in 1-3 nm was determined by evaluating the ceramic surface from various places and subsequent averaging.

### 2.2 Samples irradiation

Simulation of hydrogenation processes as a result of implantation of protons into the structure of surface layer was conducted by irradiating ceramics with protons with an energy of 1.5 MeV and a dose of  $10^{16} \text{ cm}^{-2}$  at the UKP-2-1 electrostatic accelerator (Almaty, Kazakhstan) [46]. Irradiation was done in vacuum, on a water-cooled target to reduce the possibility of thermal annealing of defects as a result of heating of the target during irradiation. Targets of 25  $\mu\text{m}$  thick were fabricated for irradiation. The choice of the target thickness for irradiation is based on the maximum path length of protons with a given energy determined using the SRIM Pro 2013 program. In this case, the use of a target thickness of 25  $\mu\text{m}$  makes it possible to evaluate structural changes along the entire proton path. The projected range in the case of protons with an energy of 1.5 MeV in AlN ceramics with a density of  $3.26 \text{ g/cm}^3$  according to calculations of the SRIM Pro 2013 program code was 20.5  $\mu\text{m}$ , energy losses  $dE/dx_{\text{electr}} = 47.8 \text{ keV}/\mu\text{m}$ ,  $dE/dx_{\text{nucl.}} = 0.03 \text{ keV}/\mu\text{m}$ . The calculation was conducted using the quick KP model, the displacement energies were selected according to the model used for calculations [47-49].

### 2.3 Isochronous thermal annealing of irradiated samples

An analysis of the influence of the possibility of using high-temperature

annealing on the partial annihilation and relaxation of defects arising during irradiation and subsequent accumulation of defects in ceramics structure, and the possibility of simulating annealing processes under real conditions of reactor materials was conducted in a muffle furnace. Isochronous annealing temperatures were 500, 600, and 700°C, and the heating rate was 20°C/min. The annealing time is 1 hour, after which the samples were cooled down together with the oven to room temperature for 8-10 hours. The choice of annealing temperatures was based on standard techniques for annealing defects at temperatures of 0.2-0.3  $T_{\text{melting}}$ . In our case, for AlN ceramics, the value  $T_{\text{melting}}=2200^{\circ}\text{C}$ . Also, the annealing temperatures were  $500^{\circ}\text{C} = 0.22 T_{\text{melting}}$ ,  $600^{\circ}\text{C}=0.27 T_{\text{melting}}$ ,  $700^{\circ}\text{C}=0.31 T_{\text{melting}}$ . For annealing, a series of samples were selected, which were irradiated under the same conditions.

#### *2.4 Study of the dynamics of changes in samples deformation*

Assessment of structural changes, including density, porosity, degree of structural ordering, and deformation of the crystal lattice was carried out by changing and fully profile analyzing X-ray diffraction patterns obtained using the X-ray diffraction method performed on a D8 Advance Eco (Bruker, Karlsruhe, Germany) instrument. X-ray diffraction patterns: Cu-k  $\lambda = 1.54 \text{ \AA}$ ,  $2\theta = 20-75^{\circ}$ , in increments of  $0.01^{\circ}$ , standing time at the point 1 sec.

The crystal lattice parameters were determined using the DiffracEVA and TOPAS v.4 software codes, which are used to interpret X-ray diffraction patterns, and to determine changes in structural parameters.

The determination of the crystallite sizes ( $L$ ) was carried out using the Williamson-Hall method [50].

The dislocation density ( $\delta$ ) was calculated by the formula (1) [35, 46]:

$$\delta = \frac{1}{L^2}, \quad (1)$$

Study of changes in surface deformation, and kinetics of changes in structural defects and surface roughness as a result of irradiation and subsequent annealing, was conducted using the atomic force microscopy method performed using the AIST-NT SPM microscope.

#### *2.5 The study of mechanical and strength properties*

The microhardness was assessed using the microindentation method with a variable load varying from 10 to 1000 N. The Vickers pyramid (a tetrahedral diamond pyramid with an angle of  $136^{\circ}$  between opposite faces) was used as an indenter. The samples were polished to reduce the ceramics thickness to determine the change in microhardness values at a depth of more than 10-15 microns.

The study of resistance to cracking and deformation of ceramics before and after external influences (irradiation, thermal annealing) was carried out by tests for wear resistance at a load of 100 N, bending strength and impact strength before and after irradiation.

Determination of strength properties was carried out using standard three-point bending strength and impact toughness test methods. For flexure tests, ASTM D790 was used to determine the modulus of elasticity and shear. The tests

were carried out at room temperature. Impact strength was determined using Charpy Impact Test Method according to ASTM E23.

### 3. Results and discussion

#### 3.1 Study of changes in structural parameters

Figure 1 shows the X-ray diffraction data of the studied ceramics before and after irradiation, and after thermal annealing.

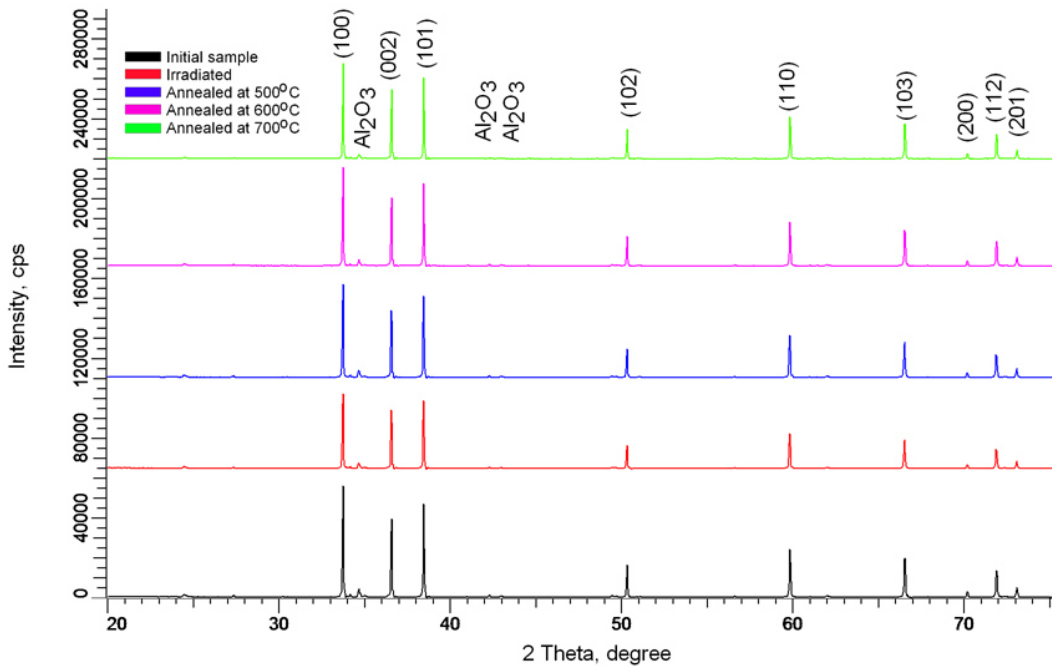


Figure 1. X-ray diffraction pattern of the AlN ceramic samples.

According to the presented data, the ceramic structure is characteristic of the hexagonal type of crystal lattice, similar to wurtzite, with the three most intense peaks at  $2\theta = 33.4^\circ$ ,  $2\theta = 36.2^\circ$  and  $2\theta = 38.1^\circ$  to which the Miller indices (100), (002) and (101) correspond respectively. In this case, a change in the position and shape of the (100) and (101) diffraction maxima corresponds to deformation or structural changes along the crystallographic axis  $a$ , and a change in the (002) diffraction maximum reflects changes along the  $c$  axis in the hexagonal lattice [15, 52]. The general view of X-ray diffractograms of irradiated and subsequently annealed samples indicates the absence of any phase transformations or the nucleation of new phases as a result of external influences. The main changes are associated with changes in intensities and positions of the diffraction lines, which indicates a distortion of the crystal structure after irradiation.

As previously shown [15, 51], the main structural changes are most pronounced in data change in the diffraction reflections. Therefore, Figure 2 shows the dynamics of change in these reflections depending on external influences. The choice of a detailed analysis of the three reflections (100), (002) and (101) presented in Figure 2 is based on the fact that these reflections most fully reflect the change in parameters of the crystal lattice as a result of external influences.

A change in their intensities, and reflections shape, indicates not only a change in defects concentration and distortions in the lattice, but also the orientation of grains (degree of texturing).

According to the technological process for producing aluminum nitride ceramics by sintering from powders, stabilizers based on powders of aluminum oxide ( $\text{Al}_2\text{O}_3$ ) or yttrium oxide ( $\text{Y}_2\text{O}_3$ ) in a percentage ratio of not more than 3-4% are used to stabilize ceramics and increase its resistance to external influences. According to the results of X-ray diffraction, low-intensity peaks at  $2\theta=34.8^\circ$ ,  $2\theta=42.1^\circ$  and  $2\theta=43.1^\circ$  are characteristic of the  $\text{Al}_2\text{O}_3$  phase, the content of which is no more than 3.7% in the structure (inset in Figure 1), which is in good agreement with passport data of the studied samples taken from the manufacturer’s website [52]. We also previously established [15, 51] that the distribution of the impurity stabilizing phase in structure is isotropic over the entire volume of the ceramic.

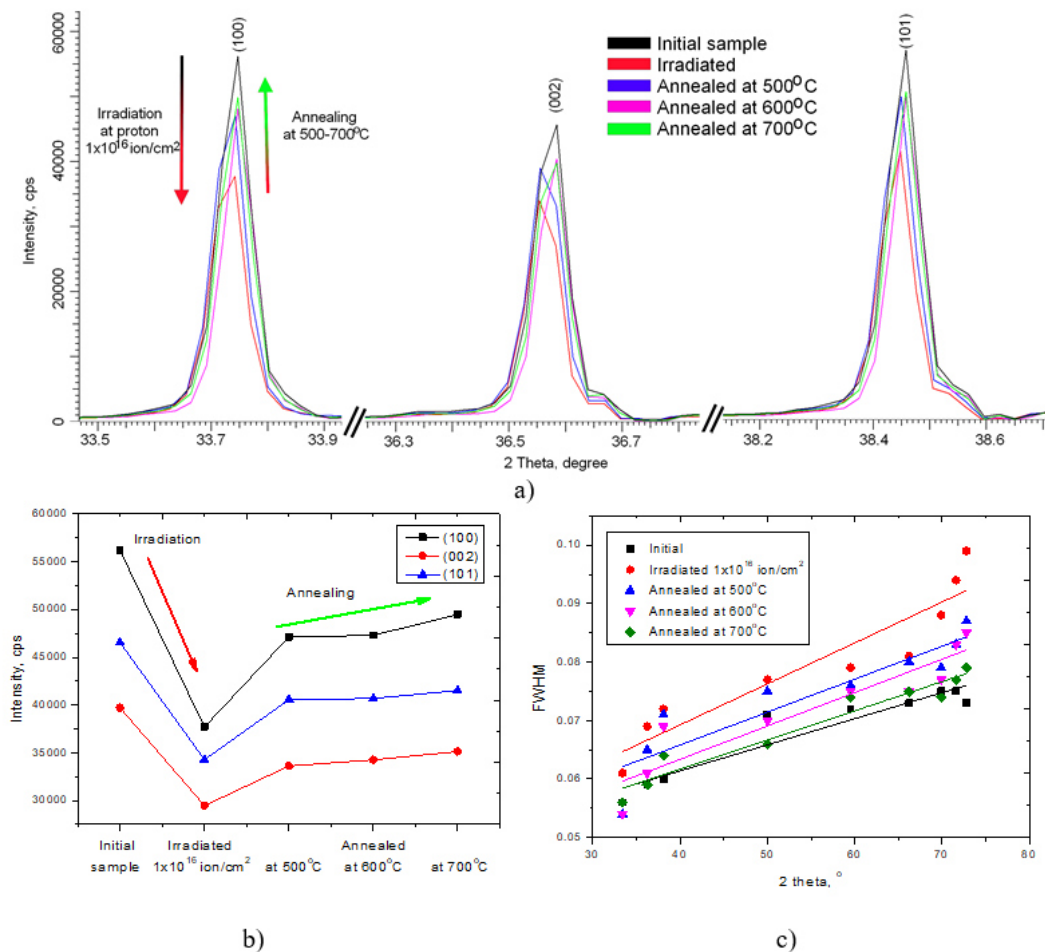


Figure 1. a) Dynamics of the main diffraction reflections (100), (002) and (101) in case of irradiation and subsequent thermal annealing; b) Graph of changes in the intensities of the main reflections (100), (002) and (101) as a result of external influences; c) Plotting angular dependencies of FWHM according to the Williamson-Hall method.

As can be seen from the data presented in Figure 2, the change in the main diffraction peaks as a result of irradiation is associated with a decrease in reflections intensity, and their shift to the region of small angles, which indicates deformation and an increase in interplanar distances. Figure 2b shows the data

on changes in intensities of the main reflections after irradiation and subsequent annealing. According to the data presented, irradiation with protons with a dose of  $10^{16} \text{ cm}^{-2}$  leads to a decrease in intensities by 25-30% of the initial value, while thermal annealing leads to a restoration of the intensity value within 84-88% of the initial value. A change in intensities indicates a change in structural distortions and deformations during annealing. The evaluation of the size factor and deformation factor affecting the distortion of diffraction reflections was carried out using the Williamson-Hall method [50], by plotting the angular dependence of the change in the width at half maximum (FWHM) of diffraction reflections in the entire considered range. Figure 2c shows the obtained dependences for all observed samples. According to the data presented, a small change in the initial position indicates a small contribution of the size factor associated with a change in the crystallite size as a result of external influences, while a change in the tilt angle for an irradiated sample is caused by an increase in distortions of the crystal structure. A decrease in the tilt angle for irradiated samples indicates a decrease and partial relaxation of distorting factors in the lattice structure.

In this case, the largest changes are observed for the (002) reflection, which indicates a large lattice deformation along the *c* crystallographic axis (see the data in Table 1, Distortion parameters along the *a* and *c* axis). In the case of annealed samples, with an increase in the annealing temperature, a partial structural ordering is observed, and an increase in reflections intensities and their shift toward large angles. That indicates the annihilation of radiation defects and partial relaxation of distortions. It is worth noting that all changes in diffraction reflections are mainly associated with the deformation and distortion of interplanar spacings and the crystal lattice, since the change in grain size as a result of irradiation and subsequent annealing is no more than 1-3%, which is within the margin of error. In this case, the dislocation density also has small changes, both as a result of irradiation and during subsequent annealing.

The degree of structural ordering (degree of crystallinity) was determined by approximating X-ray diffractograms using pseudo-Voigt functions, followed by determining the background contribution and calculating the area of reflections and amorphous halos. The value is presented in Table 1. According to the data obtained, the change in the degree of crystallinity in the case of irradiation was no more than 4-5%, while isochronous thermal annealing at a temperature of 700°C made it possible to reduce the contribution of defect regions by 4 times and to increase the degree of structural ordering by 2%.

Figure 3a shows the dynamics of changes in macrostresses resulting from distortion and deformation of interplanar spacings. The magnitudes of macrostresses were estimated on the basis of an analysis of the displacement of the three most intense diffraction reflections characterizing a change in the positions of interplanar spacings in the structure of ceramics (2) [53]:

$$\text{macrostrain} = \frac{d_{exp} - d_{pristine}}{d_{pristine}}, \quad (2)$$

where  $d_{pristine}$ ,  $d_{exp}$  are the values of the interplanar distances of the initial sample and subject to external influences. The bond length in the Al-N crystal

Table 1.  
Characterization of samples.

Parameter	Initial sample	$10^{16}$ ion/cm <sup>2</sup>	Annealing		
			500°C	600°C	700°C
Lattice parameter, Å	a=3.0956±0.0012, c=4.9557±0.0015, c/a=1.6011	a=3.1001±0.0021, c=4.9749±0.0039, c/a=1.6054	a=3.0991±0.0014, c=4.9712±0.0011, c/a=1.6047	a=3.0972±0.0019, c=4.9644±0.0013, c/a=1.6038	a=3.0967±0.0011, c=4.9611±0.0015, c/a=1.6021
	Crystalline size, nm	110±2	107±3	108±2	108.5±2
Dislocation density, 10 <sup>15</sup> unit/cm <sup>2</sup>	0.082	0.087	0.086	0.084	0.083
Distortion along the a axis	-	0.00142	0.00111	0.00048	0.00032
Distortion along the c axis	-	0.00387	0.00313	0.00176	0.00109
Defect concentration, %	0.001	0.072	0.054	0.037	0.015
Degree of structural ordering, %	97.3±1.3	93.1±1.2	93.5±1.4	94.7±1.1	95.1±1.2

lattice was determined using formulas (3-4) [54]:

$$L = \sqrt{\frac{a^2}{3} + \left(\frac{1}{2} - u\right)^2} c, \quad (3)$$

$$u = \frac{a^2}{3c^2} + 0.25, \quad (4)$$

where  $a$ ,  $c$  are the lattice parameters. Figure 3b shows the results of changes in the density of ceramics and Al-N bond lengths as a result of external influences.

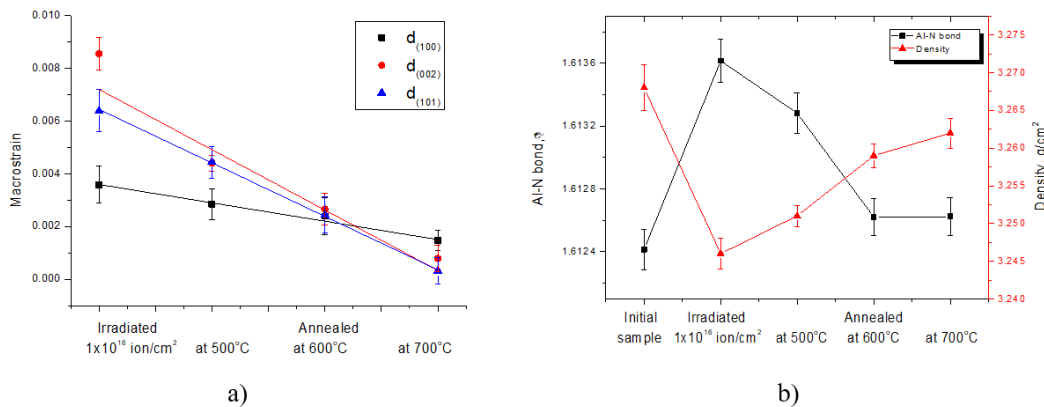


Figure 3. a) Macrostrain dynamics of interplanar distances for reflections (100), (002) and (101); b) The dynamics of changes in the density and length of the Al-N bond as a result of external influences (irradiation and subsequent thermal annealing).

According to the data presented, an increase in the annealing temperature leads to a decrease in macrostresses and strain in the structure, with the largest change being observed for the (002) and (101) planes. The formation of distortions and deformations in structure leads to the appearance of porous inclusions, and gas-filled regions with implanted hydrogen [55, 56], which leads to a decrease in density and an increase in Al-N bond lengths. However, temperature annealing leads to partial relaxation of defects, which has a positive effect on the increase in ceramics density, which amounted to 99.7 and 99.8% of the initial value for annealed at 600 and 700°C, respectively.

### 3.2 Research of strength characteristics

One of the important characteristics of ceramics considered as candidates for structural materials is not only the stability of the crystal structure to radiation, but also strength characteristics such as microhardness, bending strength, dry friction coefficient, etc. Irradiation can initiate degradation processes of the structure, which have a significant effect on the strength characteristics, and the dynamics of their change indicates ceramics resistance to irradiation.

Figure 4 presents the results of a study of changes in strength characteristics, such as depth microhardness and dry friction coefficient as a result of cyclic friction tests.

According to the obtained data, proton irradiation with a dose of  $1 \times 10^{16}$  ion/cm<sup>-2</sup> leads to a decrease in the microhardness down to a depth of 22-23  $\mu\text{m}$ . That slightly exceeds the calculated value of the maximum path length of protons in ceramics. Such a discrepancy may be due to cascading effects of

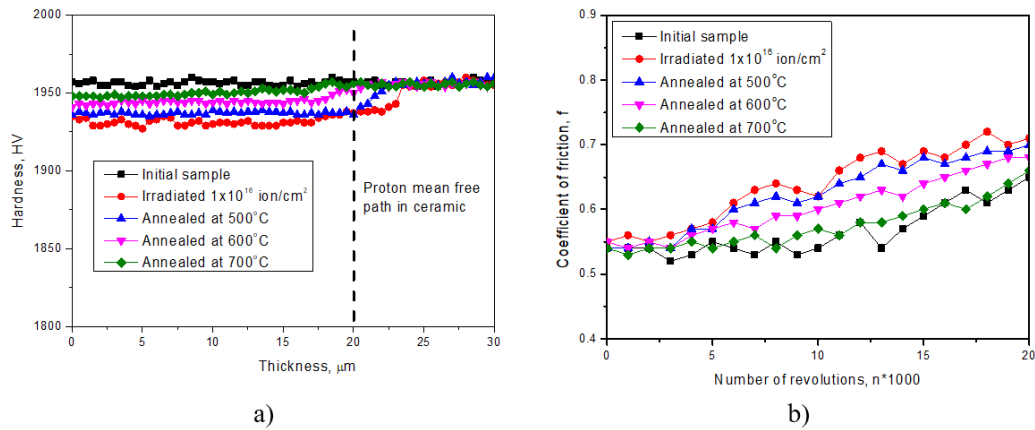


Figure 4. a) Dynamics of changes in the microhardness along the depth of studied ceramics before and after external influences; b) Dynamics of the dry friction coefficient.

defects accumulation in the structure at high radiation doses and their subsequent migration in the ceramic structure to a greater depth exceeding the maximum path depth. In the case of annealed samples, not only an increase in the microhardness is observed. But also a decrease in the damage thickness is observed that indicates the relaxation nature of removal of distortions and deformations in the structure. In the case of wear tests, changes in the coefficient of dry friction for the initial sample are a slight increase (not more than 10-15%) after 10,000 test cycles, which is due to slight damage to surface layer structure as a result of friction. For irradiated samples, an increase in the dry friction coefficient is observed after 5000-7000 test cycles, which is due to the degradation of the surface layer as a result of swelling and degradation. In this case, irradiation leads to surface wear and partial cracking after testing, as evidenced by the results of Figure 5a. For annealed samples, the change in the value of the dry friction coefficient decreases, and at a temperature of 700°C, the value of the coefficient is comparable with the value for the initial sample.

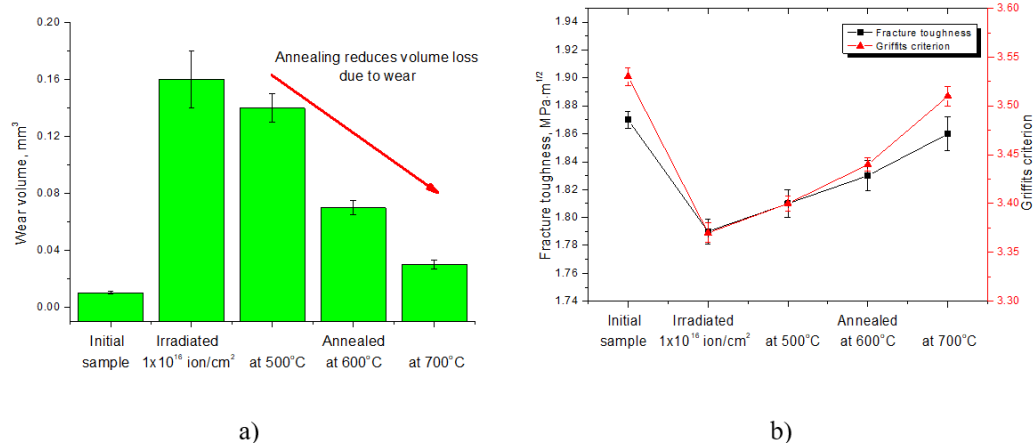


Figure 5. a) Diagram of changes in ceramics wear for all considered cases; b) Dynamics of change of fracture viscosity coefficient and crack resistance coefficient of ceramics.

Figure 5b presents the results of changes in values of the fracture toughness coefficient and the Griffiths criterion. Determination of the fracture toughness coefficient of the surface layer subjected to irradiation and subsequent thermal annealing was carried out using formula (5) [57, 58]:

$$K_{IC} = 0.016 \left( \frac{E}{H} \right)^{0.5} \frac{P}{c^{1.5}}, \tag{5}$$

where  $E$  is Young's modulus ( $Y=308$  GPa [59] ),  $H$  is microhardness,  $P$  is load force,  $c$  is crack size.

The study of the criterion of resistance to fracture was determined using the Griffith criterion, which characterizes the degree of structural deformation and resistance to cracking as a result of external influences (6) [57, 58]:

$$K_{cr} = S^2L, \tag{6}$$

where  $S$  is the average stress,  $L$  is the crystallite size.

According to the data presented in Figure 5b, thermal annealing leads to a significant decrease in the effect of radiation damage, and an increase in the crack resistance of ceramics to external influences.

Table 2 presents the results of changes in strength characteristics, such as bending strength and viscosity parameters, according to which it is clear that thermal annealing leads to a partial recovery of strength characteristics at a temperature of 500-600°C, and in the case of 700°C, the strength parameters are close to the original values within the error. The positive dynamics of changes in the strength characteristics of annealed ceramics indicates the promise of using thermal annealing for partial relaxation and removal of deformations in the structure, which can significantly increase the time of ceramic exploitation in the future.

Table 2.  
Data of strength parameters.

Parameter	Initial sam- ple	10 <sup>16</sup> ion/cm <sup>2</sup>	Annealing		
			500°C	600°C	700°C
Three-point bending strength (MPa)	164±3	155±2	157±3	160±1	163±2
Impact tough- ness (kJ/mm <sup>2</sup> )	1.41±0.09	1.32±0.04	1.35±0.03	1.38±0.04	1.40±0.02

### 3.3 Study of changes in surface morphology

Figure 6 shows the dynamics of surface morphology of studied ceramic samples before and after irradiation and subsequent thermal annealing obtained using the atomic force microscopy method by constructing 3D images of the surface morphology. Small defects in the form of scratches and small tubercles on the initial sample surface are due to sample preparation in the form of grinding using abrasive materials.

Analysis of changes in the surface morphology showed that in the case of irradiated samples, the formation of defective regions is observed. These are hillocks or gas-filled sphere-like inclusions, the presence of which is characteristic of structural defects caused by irradiation. The formation of such areas is due

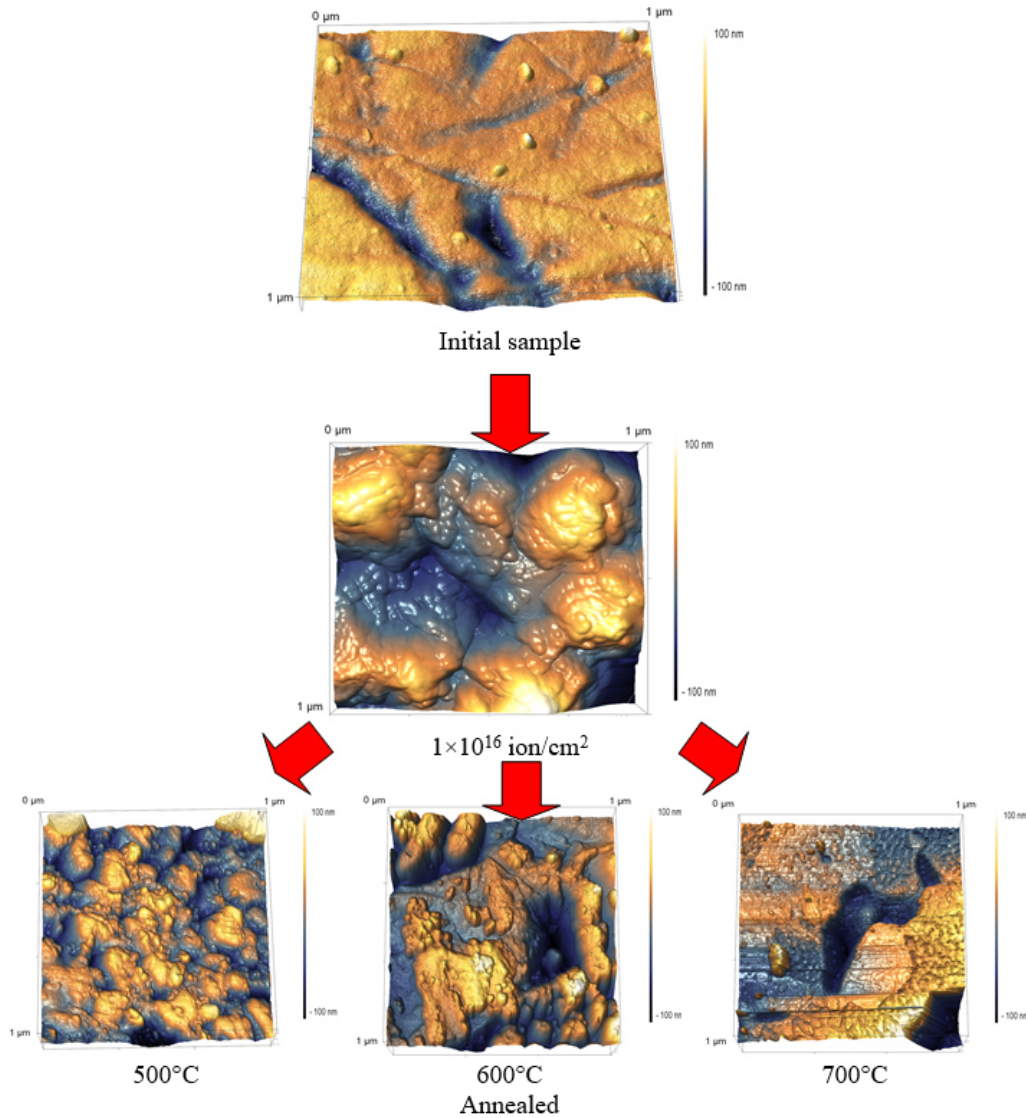


Figure 6. Dynamics of changes in the surface morphology of ceramics [the image data for the initial and irradiated sample were taken from [46].

to the partial extrusion of defects and gas inclusions to defects sinks and their subsequent migration to the surface. An increase in defects near drains and grain boundaries, and poor solubility of hydrogen, leads to the formation of highly disordered regions containing a large number of structural stresses that can squeeze the defective volume to the surface. Also, a change in defects concentration in the structure of the surface layer, and an increase in overstresses and deformations, can lead to partial cracking and peeling of the surface layer. This also negatively affects the operation properties of ceramics. Moreover, in the case of irradiated samples, the formation of clusters of hillocks consisting of several sublayers is observed. The presence of such a complex structure of hillocks is due to the effects of overlapping of defective regions at high radiation doses.

Paper [60] proposed a detailed scheme for the formation of hillocks in films based on zirconium, aluminum, and chromium nitrides, according to which the formation of hillocks or gas-filled blisters occurs as a result of defects accumula-

tion near defect sinks and grain boundaries. In the case of prolonged irradiation leading to distortion and deformation of the crystal structure, which leads to the formation of cavities, which in the layer can be filled with intercalated ions capable of forming cluster inclusions with excess pressure. An increase in excess pressure can lead to partial swelling, and squeezing out the volume to the surface, which leads to hillocks or blisters formation.

The second reason for the change in the surface as a result of irradiation is processes of partial sputtering and peeling of the near-surface layer after irradiation. These effects are mainly observed at irradiation with low-energy gas ions or fast heavy ions [51, 60-62]. In this case, deformation occurs as a result of a large amount of transferred kinetic energy into the electronic and nuclear subsystem of the target, which leads to the appearance of a large number of initially knocked-out atoms, and electron cascades capable of significantly deforming the structure.

For annealed ceramics, a decrease in the density of defective inclusions and their size is observed, which indicates partial relaxation of defects as a result of annealing. Moreover, the greatest smoothing of the surface occurs at an annealing temperature of 700°C. At this temperature, a decrease in the area and size of hillocks is observed, and the main surface damage remains only in the form of exfoliation of the surface layers.

The maximum stress arising in defective areas on the surface of irradiated and subsequently annealed ceramics was calculated as a function of pressure using formula (7) [16]:

$$\sigma^{2D} = \sqrt{\frac{prE}{2}}, \quad (7)$$

where  $E$  is Young's modulus [60],  $r$  is the radius of the hillock,  $p = \rho RT$  pressure. The results of magnitude change of stresses arising in hillocks, and the percentage of the damaged surface area are presented in Figure 7.

According to the data presented, temperature annealing leads to partial stress relief, and relaxation of the most defects in surface layer, which leads to relaxation of distortions and partial ordering. The presented data on the degree of surface erosion in Figure 7a indicate that irradiation leads to damage to about 80% of the entire ceramic surface, due to hillocks formation, and partial swelling of sample after of defects accumulation. Thermal annealing leads to a decrease in the degree of surface erosion; however, according to the data of atomic force microscopy, large craters and hollows are formed on ceramic surface, which are characteristic of the processes of peeling off damaged layers. The processes of peeling off the damaged surface during thermal heating can be due to the fact that, if the annealing temperature is increased, additional thermal vacancies appear in the structure, which can cluster with radiation defects and intercalated hydrogen. The formed clusters can dramatically increase the pressure in cavities, which leads to their destruction and flaking. The migration of thermal vacancies and clusters formation, followed by exfoliation, leads to a decrease in defects concentration and stabilization of the crystal structure throughout the sample.

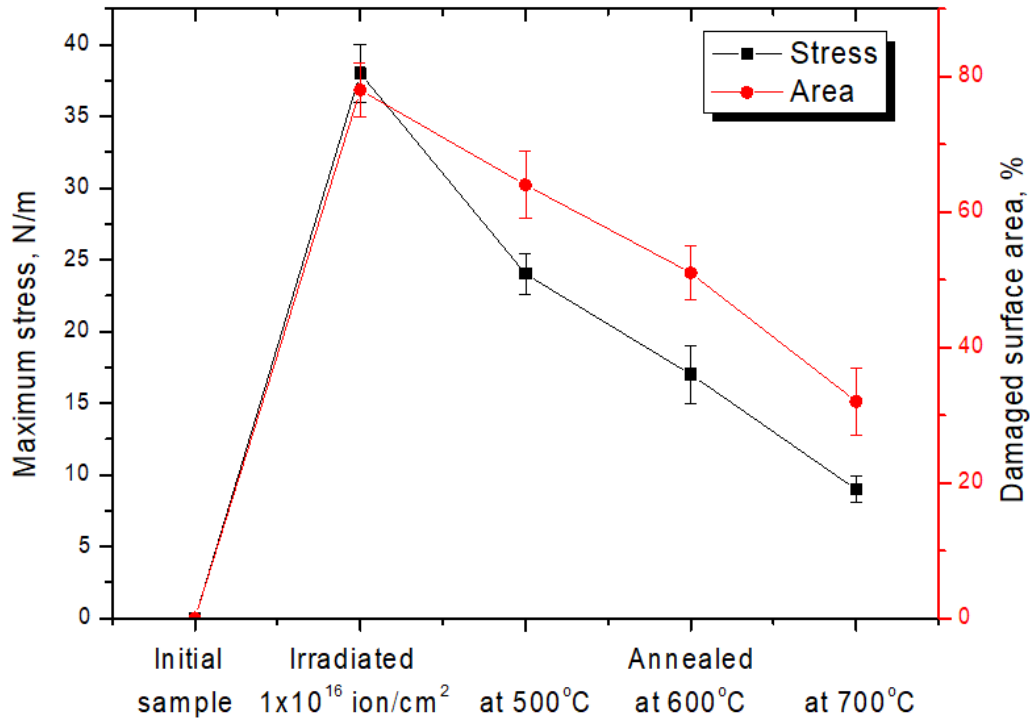


Figure 7. a) Graph of changes in the stress value in defective areas and the area of the damaged surface of ceramics; b) Graph of changes in defects density on ceramics surface.

### 3.4 Discussion of the obtained results and mechanisms of defects annealing

As a rule, post-radiation annealing of defects is used to anneal point defects and vacancies, and partial relaxation of defects in steels, crystals, and ceramics exposed to irradiation. A change in structural and mechanical properties occurs as a result of the emergence in material structure of non-equilibrium processes associated with the formation and subsequent accumulation of vacancies and point defects. In this case, the annealing temperature is selected so that the thermal energy is sufficient for annealing the defects, but at the same time insufficient for the formation of new defects as a result of thermal heating.

In general, the process of defects thermal annealing can be described by the following formula (8) [63]:

$$\frac{dn}{dt} = -nv(-\Delta E_a/kT), \quad (8)$$

where  $n$  is defects concentration in the structure,  $v$  is the frequency of thermal vibrations of atoms in the crystal lattice,  $\Delta E_a$  is the activation energy of defects annealing,  $k$  is the Boltzmann constant, and  $T$  is the annealing temperature. In this case, when the value of  $\Delta E_a$  is sufficiently small, annealing of defects does not occur, and the formed defects remain stable, despite the fact that they are in a non-equilibrium state. An increase in the annealing temperature leads not only to an increase in thermal vibrations, but also to an increase in the degree of mobility of point defects and vacancies in the structure. In the case of isochronous annealing at low temperatures, only the processes of recombination of interstitial sites and vacancies located close to each other are possible, which leads to a

small annealing effect. The main process of recombination in this case is due only to the mobility of interstitial atoms over small distances. An increase in the annealing temperature can lead to the fact that interstitial atoms go to more sinks to the grain boundaries. In this case, dislocations in the structure can be annealed, and the grain size can also change. A further increase in the annealing temperature, as a rule, leads to the processes of decay of cluster defects, and the liberation of interstitial atoms from traps with subsequent recrystallization and phase transformations. In our case, according to the data obtained, the presence of new phases, and processes of recrystallization associated with an abrupt change in grain sizes, was not observed. That indicates that the main processes during post-radiation annealing in a given temperature range are associated with the recombination of point defects, and their annealing of dislocations. A change in defects concentration as a result of an increase in the annealing temperature leads to a decrease in the anisotropic distortion of the crystal lattice, and to an increase in the degree of perfection of the crystal structure.

In most cases, thermal annealing is used to restore radiation damage, in order to increase the operation life, and to preserve the characteristics of the material. For example, in [64] it was shown that in the case of post-radiation annealing of AlN ceramic samples irradiated with neutron fluxes, an increase in the annealing temperature led to a decrease in the anisotropy of the crystal lattice swelling. Also, the authors showed that the level of ceramics swelling a result of irradiation at higher temperatures becomes less, which is due to the partial annihilation of point defects during irradiation. The behavior of changes in structural parameters, particularly, the parameters of the crystal lattice and its anisotropy, obtained in [64], are similar to the obtained temperature dependences of changes in parameters of the crystal lattice in this work. The use of isochronous annealing of radiation defects arising from neutron irradiation of AlN ceramics is shown in [65]. The authors of the work have shown that the greatest decrease in defects concentration arising during irradiation is observed when the annealing temperature exceeds 600°C. In this case, an increase in the annealing temperature above 900°C leads to an increase in linear dimensions of the samples as a result of swelling. Structural changes caused at temperatures above 900°C indicate that the selected annealing temperature range of 500-700°C in this work avoids structural changes associated with a change in linear dimensions, and in recrystallization processes. The effect of isothermal annealing of AlN ceramics samples irradiated with neutrons is considered in [66], where the authors showed that the greatest changes occur in the time period from 0 to 30–80 minutes, depending on the annealing temperature. This also has good agreement with the chosen isochronous annealing time in this work.

## Conclusion

The paper presents the results of studying of the applicability of high-temperature heat treatment (500-700°C) of nitride ceramics exposed to irradiation with protons with an energy of 1.5 MeV and a dose of  $10^{16} \text{ cm}^{-2}$ . During studies, it was found

that heat treatment for 60 minutes at a temperature of 700°C can significantly reduce the density of radiation-induced defects and distortions in ceramics structure, due to partial annihilation and relaxation of point defects. Dependences of changes in the strength and mechanical characteristics of ceramics on the temperature of post-irradiation annealing are shown. Based on the data obtained, a conclusion was made on the prospects of using post-irradiation annealing to maintain the strength of ceramics exposed to loading during operation.

## Acknowledgments

This research was funded by the Science Committee of the Ministry of Education and Science of the Republic of Kazakhstan (No. AP08051975).

## References

- [1] W. Dienst, *Journal of nuclear materials* **191** (1992) 555-559.
- [2] Azevedo Cesar Roberto de Farias. *Engineering Failure Analysis* **18**(8) (2011) 1943-1962.
- [3] B. Jean-Pierre et al., *MRS bulletin* **34**(1) (2009) 28-34.
- [4] K. Tinishbaeva et al., *Journal of Materials Science: Materials in Electronics* **31**(3) (2020) 2246-2256.
- [5] T. Yano et al., *Journal of nuclear materials* **283** (2000) 947-951.
- [6] Zhang Yongfeng, Xian-Ming Bai, *JOM* **71**(12) (2019) 4806-4807.
- [7] Ang, Caen, Lance Snead, and Yutai Kato, *Journal of Nuclear Materials* (2020) 151987.
- [8] D.L. Smith et al., *Fusion Engineering and Design* **61** (2002) 629-641.
- [9] M. Khafizov et al., *Journal of Materials Research* **32**(1) (2017) 204-216.
- [10] Q. U. A. N. L. I. Hu et al., *Radiation effects and defects in solids* **147**(4) (1999) 283-292.
- [11] Z. Rosenberg, N.S. Brar, S.J. Bless, *Journal of applied physics* **70**(1) (1991) 167-171.
- [12] S.J. Zinkle, *Structural Materials for Generation IV Nuclear Reactors*. Woodhead Publishing, 2017. 569-594.
- [13] T. Wubian, *MAX Phases and Ultra-High Temperature Ceramics for Extreme Environments*. IGI Global, 2013. 460- 477.
- [14] Yano, Toyohiko and Takayoshi Iseki, *Journal of nuclear materials* **179** (1991) 387-390.
- [15] T. Gladkikh et al., *Vacuum* **161** (2019) 103-110.
- [16] A. Kozlovskiy et al., *Vacuum* **163** (2019) 45-51.
- [17] K. Dukenbayev et al., *Journal of Materials Science: Materials in Electronics* **30**(9) (2019) 8777-8787.
- [18] T. Yano et al., *Journal of nuclear materials* **283** (2000) 947-951.
- [19] A. Kozlovskiy et al., *Materials* **12**(15) (2019) 2415.
- [20] Han Xiao, Xiguang Gao and Yingdong Song, *Materials Science and Engineering: A* **746** (2019) 94-104.

- [21] A.S. Vokhmintsev, I.A. Weinstein and D.M. Spiridonov, *Journal of luminescence* **132**(8) (2012) 2109-2113.
- [22] Hu Quanli et al., *Nuclear Instruments and Methods in Physics Research Section B: Beam Interactions with Materials and Atoms* **191**(1-4) (2002) 536-539.
- [23] Ya. Takayuki et al., *Journal of the Ceramic Society of Japan* **121**(1420) (2013) 988-991.
- [24] L. Trinkler et al., *Nuclear Instruments and Methods in Physics Research Section A: Accelerators, Spectrometers, Detectors and Associated Equipment* **580**(1) (2007) 354-357.
- [25] Ya. Toyohiko, T. Iseki, *Journal of nuclear materials* **203**(3) (1993) 249-254.
- [26] M. Akiyoshi et al., *Journal of nuclear materials* **329** (2004) 1466-1470.
- [27] W. Dienst, *Journal of nuclear materials* **191** (1992) 555-559.
- [28] T. Yano et al., *Journal of nuclear materials* **283** (2000) 947-951.
- [29] M. Milosavljevic et al., *Journal of Physics D: Applied Physics* **43**(6) (2010) 065302.
- [30] S.O. Kucheyev et al., *Journal of applied physics* **92**(7) (2002) 3554-3558.
- [31] S.J. Zinkle, V.A. Skuratov, and D.T. Hoelzer, *Nuclear Instruments and Methods in Physics Research section B: Beam Interactions with Materials and Atoms* **191**(1-4) (2002) 758-766.
- [32] Hu Xinwen et al., *IEEE Transactions on Nuclear Science* **50**(6) (2003) 1791-1796.
- [33] Z. Qiaoying, M.O. Manasreh, *Applied physics letters* **80**(12) (2002) 2072-2074.
- [34] A.L. Kozlovskiy et al., *Solid State Sciences* (2020) 106367.
- [35] A.L. Kozlovskiy et al., *Crystals* **10**(6) (2020) 546.
- [36] Yu.F. Zhukovskii et al., *Journal of Physics: Condensed Matter* **19**(39) (2007) 395021.
- [37] A. Kozo, M. Okada, and M. Nakagawa, *Nuclear Instruments and Methods in Physics Research Section B: Beam Interactions with Materials and Atoms* **166** (2000) 57-63.
- [38] A. Kozo et al., *Japanese journal of applied physics* **29**(1R) (1990) 150.
- [39] E.A. Kotomin et al., *Nuclear Instruments and Methods in Physics Research Section B: Beam Interactions with Materials and Atoms* **374** (2016) 107-110.
- [40] E. Kotomin et al., *The Journal of Physical Chemistry A* **122**(1) (2018) 28-32.
- [41] A.I. Popov et al., *Nuclear Instruments and Methods in Physics Research Section B: Beam Interactions with Materials and Atoms* **433** (2018) 93-97.
- [42] L.L. Snead, S.J. Zinkle and D.P. White, *Journal of nuclear materials* **340**(2-3) (2005) 187-202.
- [43] A.I. Popov, I. Plavina, *Nuclear Instruments and Methods in Physics Research Section B: Beam Interactions with Materials and Atoms* **101**(3) (1995) 252-254.
- [44] Soni Anuj et al., *Radiation measurements* **47**(2) (2012) 111-120.
- [45] A. Vokhmintsev, I. Weinstein, D. Spiridonov, *Physica status solidi c*, **10**(3) (2013) 457-460.
- [46] A. Kozlovskiy et al., *Journal of Materials Science: Materials in Electronics* **31** (2020) 11227-11237.
- [47] W.J. Weber, Y. Zhang, *Current Opinion in Solid State and Materials Science* **23**(4) (2019) 100757.

- [48] J.F. Ziegler, J.P. Biersack, M.D. Ziegler, SRIM: <http://www.srim.org> (2009).
- [49] E.H. Lee, Nuclear Instruments and Methods in Physics Research Section B: Beam Interactions with Materials and Atoms **151**(1-4) (1999) 29-41.
- [50] Z.A. Khorsand et al., Solid State Sciences **13**(1) (2011) 251-256.
- [51] A. Kozlovskiy et al., Vacuum **155** (2018) 412-422.
- [52] Shenzhen Jia Rifeng Tai Electronic Technology.  
<http://www.jrftdz.com/en/alnsicceramic/85-104>.
- [53] D.B. Borgekov et al., Crystals **10**(4) (2020) 254.
- [54] Taniyasu Yoshitaka, Makoto Kasu, and Naoki Kobayashi, Applied Physics Letters **79**(26) (2001) 4351-4353.
- [55] C. Ascheron et al., Nuclear Instruments and Methods in Physics Research Section B: Beam Interactions with Materials and Atoms **28**(3) (1987) 350-359.
- [56] R.A. Khmel'nitskiy et al., Vacuum **78**(2-4) (2005) 273-279.
- [57] A.S. Bakai, Materials Science Forum **123** (1993) Trans Tech Publications Ltd.
- [58] E. Feldman, N. Kalugina, O. Chesnokova, Mining of Mineral Deposits **11**(2) (2017) 41-45.
- [59] D. Gerlich, S.L. Dole, G.A. Slack, Journal of Physics and Chemistry of Solids **47**(5) (1986) 437-441.
- [60] V.V. Uglov et al., Journal of Surface Investigation: X-ray, Synchrotron and Neutron Techniques **14** (2020) 359-365.
- [61] V.V. Uglov et al., Surface and Coatings Technology **344** (2018) 170-176.
- [62] K.K. Kadyrzhanov, K. Tinishbaeva and V.V. Uglov, Eurasian Phys. Techn. J. **17**(33) (2020) 46-53.
- [63] Van Laarhoven, J.M. Peter, E.H.L. Aarts, Simulated annealing: Theory and applications. Springer, Dordrecht, 1987. 7-15.
- [64] T. Yano et al., Journal of nuclear materials **440**(1-3) (2013) 495-499.
- [65] T. Yano, H. Miyazaki, and T. Iseki, Journal of nuclear materials **230**(1) (1996) 74-77.
- [66] T. Pornphatdetaudom, T. Yano, and K. Yoshida, Nuclear Materials and Energy **16** (2018) 24-28.